Calcium Oxalate Crystals in Tomato and Tobacco Plants: Morphology and in Vitro Interactions of Crystal-Associated Macromolecules

Nikolaos Bouropoulos, Steve Weiner, and Lia Addadi*[a]

Abstract: Plants form calcium oxalate crystals with unique morphologies under well-controlled conditions. We studied the morphology of single calcium oxalate monohydrate (whewellite) crystals extracted from tomato and tobacco leaves. These crystals have a pseudotetrahedral shape. We identified the $(\bar{1}01)$, (101) or (102), $(\bar{1}10)$, and $(h\bar{k}0)$ faces as stable faces. The morphology is chiral with unique handedness. We also show that calcium oxalate monohydrate crystals isolated from tomato, tobacco, and bougainvillea leaves contain macromolecules rich in Gly, Glx, and Ser. Crystal-associated macromolecules extracted from tomato and tobacco influence the morphology of calcium oxalate monohydrate crystals grown in vitro, promoting preferential development of the {120} faces. Furthermore, crystal-associated macromolecules from tobacco promote nucleation of calcium oxalate monohydrate crystals, whereas model polypeptides do not have any significant effect on nucleation. These results imply an active role of the crystal-associated macromolecules in the formation of pseudotetrahedral shapes in vitro, and these properties may in part be responsible for the unique chiral morphology of the natural pyramidal-shaped crystals.

Keywords: biomineralization · calcium oxalate · chirality · crystal growth · morphology

Introduction

Mineral formation in plants is a widespread phenomenon. The most abundant minerals formed by plants are amorphous silica (phytoliths), amorphous calcium carbonate (cystoliths) and calcium oxalate.[1] In higher plants calcium oxalate is probably the most commonly formed mineral.[2] Calcium oxalate crystals may form in most tissues and organs such as roots, bark, stems, leaves, flowers, fruits, and seeds.[1d] The most commonly proposed function of these crystals is the storage of calcium in an insoluble form, such that the low levels of calcium required within the cell cytosol can be maintained.[1d, 3] Other functions that have been ascribed to calcium oxalate crystals in plants are those of a protective mechanism against herbivores [1d, 4] and improving the mechanical properties of the tissues.[5]

Calcium oxalate exists in two forms in plants: calcium oxalate monohydrate (COM or whewellite) and, less commonly, calcium oxalate dihydrate (COD or weddelite).[6] The crystals adopt several different morphologies. These are described as raphides, styloids, druses, crystal sand, and variously shaped prisms.[1d, 1f] Extensive morphological studies show that these morphologies are quite different from the morphologies of calcium oxalate crystals produced in vitro.[7] Furthermore, each plant species always forms crystals with the same morphologies at the same tissue site, implying that morphology is under genetic control.[1d, 1f] The amount of crystals formed at a site varies and is influenced by environmental conditions such as light intensity, temperature, and/or soil nutrients.[8]

Calcium oxalate crystals form inside the vacuoles of specialized cells called idioblasts. In some cases one crystal is formed per vacuole, whereas in other cases many crystals are formed within a vacuole. In the latter case, each crystal still forms within a membrane-delineated space, usually termed the crystal chamber.[1d, 3, 9] This microenvironment is believed to play an important role in crystal nucleation and morphology.[10]

In biomineralization, the microenvironment in which crystallization occurs is the key to exerting control over nucleation and crystal growth in mineralized tissues.[11] This is achieved by accurate design of the size and shape of the space in which the crystals form, of the chemistry and structure of the framework that delineates the space, and of the macromolecules and ions that are present in the solution within the space.[11a, 12] It has been shown in vitro that some macromolecules extracted from mineralized tissues are able to control specifically nucleation, growth and cessation of growth of crystals, provided they are in an appropriate microenvironment.[13] A study of the raphide crystal-associ-

[a] Prof. L. Addadi, Dr. N. Bouropoulos, Prof. S. Weiner
Department of Structural Biology
Weizmann Institute of Science
Rehovot 76100 (Israel)
Fax: (+972) 8-934-4136
E-mail: lia.addadi@weizmann.ac.il

  0947-6539/01/0709-1881 $ 17.50+.50/0

ated macromolecules in leaves of *Vitis* shows that there are many different glycoproteins that make up a structurally coherent organic matrix. The results suggested that the matrix is responsible for determining crystal morphology.[14] The specific functions of crystal-associated matrix macromolecules in calcium oxalate nucleation and control of morphology in plants is, as yet, unknown. This is the focus of our study.

We chose to examine the calcium oxalate monohydrate crystals extracted from tomato *(Lycopersicon esculentum)* and tobacco *(Nicotiana tabacum)* leaves. Tobacco and tomato are both members of the family Solanaceae. The crystals form inside vacuoles as accumulations of numerous individual small crystals (crystal sand); they adopt pseudotetrahedral or cordate (heart-shaped) morphologies.[15] The pseudotetrahedral shape presents a challenging conceptual problem. Because of the total lack of morphological symmetry, the crystals have a chiral morphology. Their morphological symmetry is thus lower than the monoclinic symmetry of the crystal lattice, suggesting the influence of external chiral elements on crystal growth. For more than a century this paradox has inspired studies of the exact crystal faces of these pyramids.[16] An elegant explanation, based on crystal twinning, was suggested by Cody and Horner,[15] who also studied crystals from plants belonging to this family. The crystals we observed were not, however, all twinned. Franceschi described the formation of crystal sand in *Beta vulgaris L.* leaves (sugar beet).[9] The crystals are formed in vacuoles within idioblastic cells. Membranes are synthesized in the vacuole and are organized into chambers or vesicles. Calcium oxalate precipitates within the membrane chambers.[9]

Here we identify the faces of these unusual single pyramidal-shaped calcium oxalate crystals from tomato and tobacco leaves. Our study is focused only on crystals that are shown by electron diffraction not to be twinned. We have also extracted the macromolecules associated with these calcium oxalate crystals and shown that they are able to interact specifically with growing COM crystals in vitro, and preferentially induce crystal nucleation from a supersaturated solution. These observations may explain in part the manner in which the unusual crystal morphology is achieved in vivo.

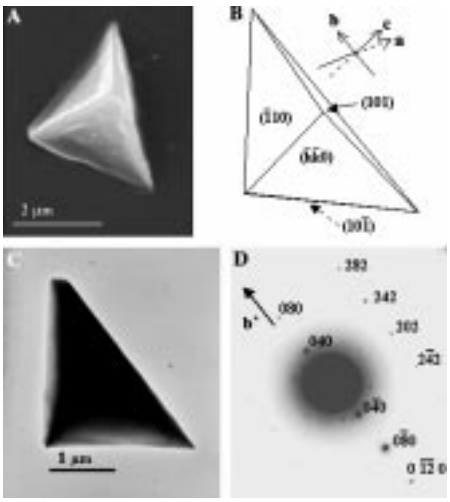

Figure 1. Morphological analyses of representative COM crystals from tomato leaves. A) SEM micrograph showing the pseudotetrahedral morphology (note that this micrograph was not taken at tilt = 0). B) Proposed morphological model based on the dihedral angle analyses (Table 1) and electron diffraction patterns. C) TEM micrograph and D) the corresponding electron diffraction pattern from the thin edge of the crystal.

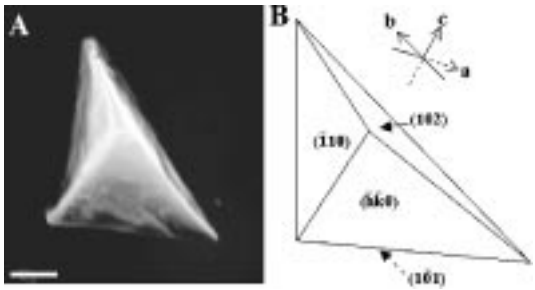

Figure 2. Morphological analyses of a representative COM crystal from tobacco leaves. A) SEM micrograph and B) proposed morphological model based on the dihedral angle analyses (Table 1) and electron diffraction patterns.

Results

Morphological analysis of natural crystals: Crystals extracted from tobacco and tomato leaves were identified as calcium oxalate monohydrate by X-ray diffraction and FTIR spectroscopy. It is important to note that indexing of the diffraction patterns, and in general any crystallographic notation, was performed using the structure of calcium oxalate monohydrate as proposed by Deganello and Piro ($P2_1/n$, $a = 9.9763$, $b = 14.5884$, $c = 6.2913$ Å, $\beta = 107.05°$).[17] Figures 1A and 2A are scanning electron micrographs representative of the crystals we chose to study, isolated from tobacco and tomato leaves respectively. They all have the pseudotetrahedral morphology and their size is between 1 – 5 μm. We stress that most of the crystals in the leaves are twinned, as noted by Cody and Horner,[15] and they often display concave dihedral angles and well-defined boundaries on the crystal faces. These properties clearly show that they are not single crystals. The crystal twinning can be easily detected by the doubling of the diffraction spots, or by the presence of two independent diffraction patterns in electron diffraction. In contrast, when smaller crystals with homogeneous morphologies were selected, electron diffraction performed at different locations on different crystal edges demonstrated that they were indeed single crystals.

Characterization of the faces of these crystals is problematic as individual crystals are too small for single-crystal X-ray diffraction analysis, but too large and hence thick for obtaining an electron diffraction pattern from an entire crystal. Furthermore, they are also beam-sensitive when examined in a TEM microscope at ambient temperatures. In the present study we combined information from dihedral angle measurements from SEM images and electron diffraction patterns taken from thin edges of the crystals maintained under cryoscopic conditions, in order to identify the dominant crystal faces. Figures 1C and D show a typical TEM image of a crystal isolated from tomato leaves and its corresponding electron diffraction pattern. The indexing corresponds to the $[10\bar{1}]$ zone axis of calcium oxalate monohydrate, showing that

0947-6539/01/0709-1882 $ 17.50+.50/0 *Chem. Eur. J.* **2001**, *7*, No. 9

the crystal lies on the $(10\bar{1})$ face. The angles of the crystal projection in the TEM correspond to the angles measured in the SEM (at tilt angle = 0).

The measured and calculated dihedral angles for crystals isolated from tomato are shown in Table 1 and the proposed morphological model is shown in Figure 1B. The differences we observed between the measured and calculated dihedral angle values are assumed to be within experimental error. When the dihedral angles are from the same pair of planes, for example between $(10\bar{1})$ and $(\bar{1}10)$, or $(10\bar{1})$ and (101), the value is the average of ten measurements. Three faces were identified unequivocally: the basal $(10\bar{1})$, (101), and $(\bar{1}10)$. The fourth face is labeled $(h\bar{k}0)$, because no solution consistent with all the measured dihedral angles could be found. We note, however, that indexing this face as $(\bar{1}\bar{2}0)$ is consistent with the dihedral angles measured for the lateral faces, albeit not with the basal face.

Table 1. Measured and calculated dihedral angles for calcium oxalate monohydrate crystals isolated from tomato and tobacco.

Tomato ($n = 5$)		
Dihedral Angle	Measured	Calculated
$(10\bar{1})$ (101)	70.4 ± 1.1	63.5
$(10\bar{1})$ $(h\bar{k}0)$	45.4 ± 5.4	–
$(10\bar{1})$ $(\bar{1}10)$	67.0 ± 4.2	73.8
$(\bar{1}10)$ $(h\bar{k}0)$	96.6 ± 2.1	104.0 *for* $(\bar{1}\bar{2}0)$
$(\bar{1}10)$ (101)	48.2 ± 1.2	54.4
(101) $(h\bar{k}0)$	69.9 ± 4.5	65.0 *for* $(\bar{1}\bar{2}0)$
Tobacco		
Dihedral Angle	Measured	Calculated
$(10\bar{1})$ (102)	50.0 ± 2.7	51.9
$(10\bar{1})$ $(h\bar{k}0)$	43.3 ± 7.6	–
$(10\bar{1})$ $(\bar{1}10)$	82.5 ± 9.1	73.8
$(\bar{1}10)$ $(h\bar{k}0)$	88.5 ± 0.8	94.2 *for* $(\bar{1}\bar{2}0)$
$(\bar{1}10)$ (102)	46.0 ± 1.4	63.3
(102) $(h\bar{k}0)$	69.0 ± 1.3	71.0 *for* $(\bar{1}\bar{2}0)$

Tobacco crystals exhibited similar morphological characteristics to those in tomato crystals, but were more heterogeneous in shape. Table 1 shows the measured and calculated dihedral angles, and Figures 2A and B show a typical SEM image of a crystal isolated from tobacco leaves and the proposed morphological model, respectively. These crystals are also characterized by having a $(10\bar{1})$ basal plane, $(\bar{1}10)$ face on the left-hand side, and an $(h\bar{k}0)$ front face. The right-hand face, however, is (102), in contrast to the tomato crystals. Our suspicion that the front face is $(\bar{1}\bar{2}0)$ was confirmed by some electron diffraction patterns taken from crystals lying on a different basal face. The larger standard deviations are attributed to the presence of minor faces, which we observed in some crystals at these locations. It is also conceivable that some crystals do have different pseudotetrahedral morphologies.

In order to verify whether the chiral crystal morphologies are racemic or enantiomerically unique, we examined more than 50 crystals from both tobacco and tomato in the SEM. These crystals all had the appropriate angles for the basal face (at 0° tilt). All of them also had the same handedness, namely the (101) or (102) face on the right side and the $(\bar{1}10)$ face on the left-hand side when observed as in Figure 1.

The crystal-associated macromolecules extracted from the calcium oxalate crystals: Table 2 shows the amino acid compositions of the total soluble matrix extracted from calcium oxalate crystals isolated from the leaves of tobacco, tomato, and bougainvillea. The last was selected as a reference for plant calcium oxalate crystals with a different morphology. In general the compositions are all similar, being dominated by hydrophilic amino acids. Interestingly, there are significant variations in the Ser and Glx contents between extracts from different aliquots of leaves. When the Ser content is high, so is the Glx content. This suggests that in the preparation procedures different proportions of Ser- and Glx-rich proteins are extracted. The total soluble protein matrix consists of 0.02 – 0.10 % of the crystal weight. The treatment of the crystals with 1M KOH at 75° C for 30 min removes all the proteins adsorbed on the surface of the crystals. The amount of proteins isolated after this treatment was 60 % of the total soluble protein, showing that the intracrystalline proteins comprise up to at least 60 % of total soluble protein.

Table 2. Amino acid compositions of the soluble proteins associated with calcium oxalate crystals isolated from tobacco, tomato, and bougainvillea leaves. Concentrations are expressed in mole %.

Sample[a]	Tobacco		Tomato			Bougainvillea
	1	4	1	2	3	1
Asx[b]	7.3	7.8	7.2	8.9	6.9	5.9
Thr	4.0	4.3	3.1	5.1	4.2	4.7
Ser	8.4	18.8	9.9	15.3	18.4	10.5
Glx[c]	12.6	17.9	11.2	14.9	17.0	10.9
Pro	5.2	3.1	6.0	4.4	3.6	4.4
Gly	17.5	17.1	21.5	16.9	17.9	17.6
Ala	12.6	10.0	10.7	8.6	10.1	12.2
Cys	–	–	–	–	–	3.0
Val	4.8	3.4	4.1	4.8	3.6	4.5
Met	1.2	0.8	4.2	1.0	0.9	0.8
Ile	3.7	2.0	5.1	3.1	1.9	3.0
Leu	6.1	2.6	5.0	5.2	2.7	4.9
Tyr	2.1	1.3	1.8	1.6	1.5	2.1
Phe	3.1	1.5	2.2	2.6	1.6	2.8
Lys	4.9	3.5	2.6	3.4	3.6	4.8
His	2.3	4.7	3.0	2.3	4.8	4.5
Arg	4.2	1.2	2.4	1.9	1.3	3.4
Weight %	0.03	0.10	0.02	0.08	0.06	0.03

[a] Each analysis is from a different aliquot of leaves. [b] Asx = combination of Asp and Asn. [c] Glx = combination of Glu and Gln.

FTIR spectra of the soluble matrices of tobacco and tomato extracts (Figure 3) show that the Amide I peak absorbs around 1630 cm^{-1}, which may indicate that a significant proportion of the proteins adopt the β-sheet composition. It is noteworthy that the Amide II absorption is absent. A similar phenomenon has been noted in mollusk shell matrix proteins.[18] The infrared spectra also show that the macromolecules extracted from the tomato crystals contain more polysaccharides (indicated by the wide band at 1050 – 1100 cm^{-1}) than those from the tobacco crystals.

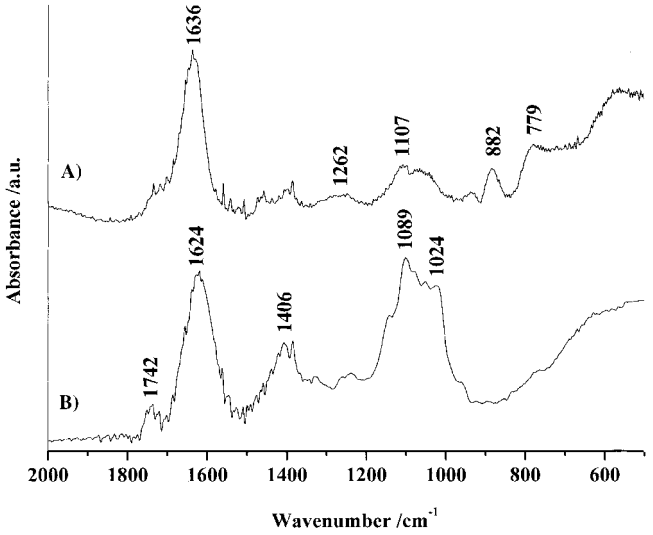

Figure 3. Infrared spectra of the soluble assemblage of crystal-associated macromolecules extracted from COM crystals isolated from A) tobacco and B) tomato leaves.

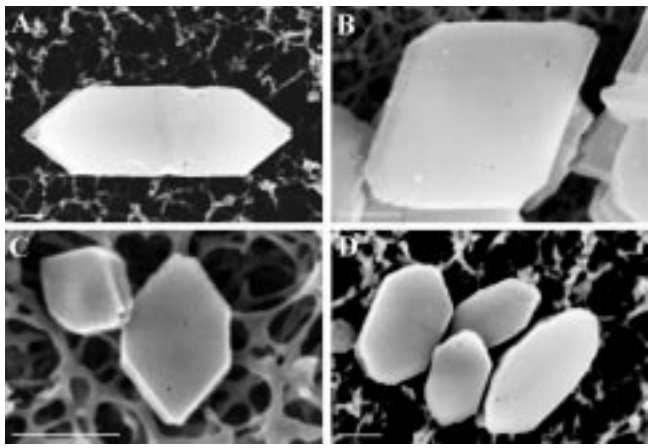

Figure 4. SEM micrographs of COM crystals grown by the diffusion technique with oxalate placed initially inside the dialysis bag. A) Control crystal grown in the absence of additives. B) Crystal grown in the presence of macromolecules extracted from tomato leaf crystals (protein concentration 15.7 $\mu g\,mL^{-1}$). C) Crystals grown in the presence of macromolecules extracted from tobacco leaf crystals (protein concentration 16.2 $\mu g\,mL^{-1}$). D) Crystals grown in the presence of macromolecules extracted from bougainvillea leaf crystals (protein concentration 17.6 $\mu g\,mL^{-1}$). Note that the crystals grown in the presence of additives are much smaller than the control crystals. Scale bars: one micron.

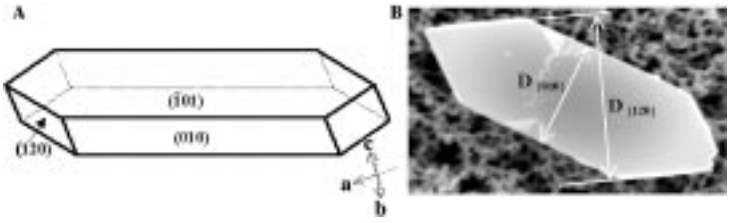

Figure 5. A) Schematic representation of the morphology of a COM crystal showing the expressed faces. B) Morphological characterization of COM crystals grown in vitro. $D_{\{120\}}$ and $D_{\{010\}}$ are the respective perpendicular distances between the edges of the {120} and {010} faces measured on the (10$\bar{1}$) plane.

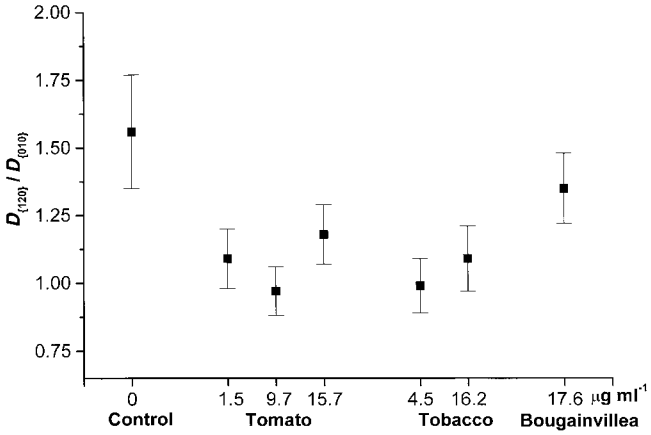

Figure 6. Effect of soluble macromolecules on the morphologies of crystals grown in the presence of various additives as expressed by the $D_{\{120\}}/D_{\{010\}}$ ratio. The lower values of the ratio compared with the controls indicate inhibition of {120} faces by the additives.

Interaction of the macromolecules with calcium oxalate crystals: Crystals of calcium oxalate monohydrate (COM) were grown by means of the diffusion growth technique in the presence of macromolecules extracted from the tomato and tobacco crystals. Bougainvillea *(Bougainvillea sp.)* macromolecules were used for comparison. Two versions of the experiment were performed: one in which the oxalate solution was placed in the dialysis bag and the calcium outside, and one in which calcium was placed inside the bag and oxalate outside. The morphologies of the crystals were then examined in the SEM. The crystals grew inside the solution and not attached to the membrane. Consistent changes in morphology in comparison with control crystals grown in the absence of matrix macromolecules are an indication of specific interactions between at least some of the macromolecules and certain faces of the growing crystals.[19] Specific effects were only obtained when the oxalate solution was placed in the dialysis bag and the calcium solution outside, indicating that the kinetic effects resulting from protein adsorption occur in excess of oxalate. The results for the oxalate-rich environment are shown in Figure 4. In all cases, crystals developed a prismatic habit with {10$\bar{1}$1}, {010}, and {120} as the principal faces. In the absence of plant macromolecular additives, the crystals were elongated along the [101] direction (Figure 4A). In the presence of the soluble matrix macromolecules the crystals were less elongated and the development of {120} faces was favored (Figure 4A – D). This implies that at least some of the macromolecules interact selectively with {120} faces. In order to quantify this effect, the ratio $D_{\{120\}}/D_{\{010\}}$ was measured in more than 30 crystals for each plant. $D_{\{120\}}$ and $D_{\{010\}}$ are the respective perpendicular distances between the edges of the {120} and {010} faces measured on the (10$\bar{1}$) plane (Figure 5). The results are shown in Figure 6. The ratios obtained from the tomato and tobacco crystals were consistently lower than those from the control and bougainvillea crystals. In all cases the values were significantly different from the control (t-test at the 0.05 level). The calcium oxalate crystals grown in the presence of matrix extracted from bougainvillea were characterized by rounded edges and stepped faces, indicating nonspecific inhibition of crystal growth in all directions. Interestingly,

0947-6539/01/0709-1884 $ 17.50+.50/0 *Chem. Eur. J.* **2001**, *7*, No. 9

the effect is not concentration-dependent, indicating that low macromolecular concentrations lead to maximal selective adsorption, above which nonspecific adsorption on all faces occurs.

Effect of the crystal-associated macromolecules on calcium oxalate monohydrate nucleation: The diffusion growth experiments described above also indicated that the assemblages of macromolecules from the tobacco and tomato crystals had an effect on the nucleation of the crystals, in that more and smaller crystals (Figure 4) were nucleated in the presence of the protein than in the controls. In order to verify this nucleation effect, we performed spontaneous precipitation experiments in the presence and absence of macromolecules. The nucleation effect is expressed as t_o/t_i, where t_o is the induction time for crystallization in the absence of additive, and t_i the induction time in the presence of the additive. The induction time was measured as the time elapsed between the creation of the supersaturation conditions and the appearance of turbidity in the solution, measured by absorbance (620 nm). According to classical nucleation theory the induction time is inversely proportional to the nucleation rate.[20] The influence of macromolecules extracted from tobacco and three control polypeptides (BSA, polyaspartic acid, and polylysine) on COM nucleation is shown in Figure 7.

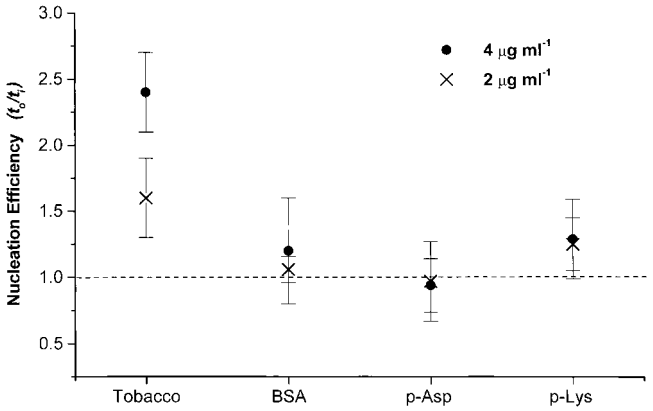

Figure 7. Effect of soluble macromolecules and polypeptides from tobacco on COM nucleation at two different concentrations. t_o = induction time for crystallization in the absence of protein. t_i = induction time for crystallization in the presence of protein. Values of the ratio $t_o/t_i > 1$ thus show promotion of nucleation, whereas values < 1 show inhibition.

Tobacco-soluble matrix at a concentration of 4 μg mL^{-1} increases the nucleation efficiency by about 2.5 times compared with the three controls. The increase in nucleation efficiency of the tobacco macromolecules at a concentration of 2 μg mL^{-1} is also significantly greater than the controls.

Discussion

We have shown that calcium oxalate monohydrate crystals extracted from tomato and tobacco leaves exhibit a pyramidal morphology delimited by $(\bar{1}01)$, (101) or (102), and $(\bar{1}10)$ faces. The fourth face was indexed in both cases as $(h\bar{k}\bar{0})$, and is most probably $(\bar{1}\bar{2}0)$. In no case were the enantiomorphous morphologies observed (namely $(10\bar{1})$, $(\bar{1}0\bar{1})$, $(1\bar{1}0)$, and $(hk0)$), or could the data be fitted to any alternative combination of faces with opposite handedness. The(101) or (102) faces are not normally expressed in calcium oxalate monohydrate crystal morphology, implying that they are somehow stabilized in the environment of the plant vacuoles. We have also shown that the assemblage of macromolecules associated with these crystals is able in vitro to promote nucleation of calcium oxalate monohydrate. Some or all of these macromolecules are able to interact in vitro with the (120) face of growing COM crystals.

Calcium oxalate monohydrate crystallizes in the monoclinic space group $P2_1/n$.[17] In this centrosymmetric space group there is a center of inversion, and in theory the crystals should express the symmetry-related faces. The fact that the symmetry-related faces, for example (120) and $(\bar{1}\bar{2}0)$, are not developed in these crystals is an indication that some chiral external factor is determining their morphology. The individual crystals do grow in specialized chambers, and it may well be that the shape and the structure of the surfaces of these chambers are important in determining the precise crystal morphologies.

A conceivable scenario in agreement with all the reported data is that nucleation of the biogenic crystals occurs within the vacuoles selectively from the normally unexpressed planes, (101) for tomato and (102) for tobacco. The reduction in symmetry would then be determined during the nucleation step, by macromolecules on the vacuole wall surface, that are able to distinguish between the opposite sides of the same plane. The crystals would then grow "normally" by completing their morphology with the development of faces that, by and large, crystals grown from standard solutions also develop (namely $(\bar{1}01)$, $(\bar{1}10)$, and $(\bar{1}\bar{2}0)$). We note that nucleation from these planes may also occur in the twinned crystals, even though we have not identified the faces developed in these crystals. It is especially interesting that the putative nucleation plane is the only one that is developed with different indices in the two plants, thus suggesting precise genetic control. Analogous phenomena of reduction in morphological symmetry have been observed in biogenic crystals in sponge spicules,[21] coccoliths,[22] and the magnetite crystals formed by magnetotactic bacteria.[23] In molecular crystals, reduction in morphological as well as in lattice symmetry through additive incorporation has been demonstrated.[24] Some of these examples may be explained by enantioselective nucleation, others would be better explained by enantioselective adsorption during crystal growth. The adsorption of antifreeze proteins to certain faces of ice crystals, but not to the symmetry-related faces, is another example of enantioselective adsorption in nature.[25]

Calcium oxalate crystals isolated from tomato and tobacco leaves contain very small amounts of crystal-associated macromolecules, namely up to 0.1 weight percent protein. These macromolecules are presumably located both on the crystal surface and within the crystal itself. This amount of protein is comparable to the total intracrystalline matrix content of sea-urchin skeletons [26] and mollusk shells.[27] In contrast, the amount is very low compared with the matrix

contents of calcium oxalate stones, which can reach 2–5% of the total weight.[28] The amino acid compositions of the matrix protein assemblages in tomato and tobacco crystals are rich in Gly, Glx, and Ser. This composition is similar to that of the protein assemblage extracted from amorphous calcium carbonate of ascidian antler spicules and the amorphous calcium carbonate layer of triradiate sponge spicules.[29] Most of the macromolecules found in urinary stones and many other nonpathological mineralized tissues are rich in aspartic acid and often phosphorylated residues as well.[28a, 30] Recently the first basic protein in calcium oxalate stones was reported.[31] Webb et al.[14] demonstrated by gel electrophoresis that there are many different crystal-associated macromolecules in raphides in grape leaves, and that they are generally glycosylated.

We have shown here that the assemblage of crystal-associated macromolecules from tobacco leaves promotes nucleation of calcium oxalate in vitro. In contrast three model polypeptides, polyaspartate, polylysine, and bovine serum albumin, do not have any significant influence on nucleation. The role of macromolecules in nucleation is variable. They may have a dual function as promoters when adsorbed on surfaces, or as inhibitors when present in solution [32] The protein albumin has a polyelectrolyte character due to the presence of relatively large numbers of acidic and basic residues on its surface. It is reported to act as a promoter of nucleation of calcium oxalate crystals at concentrations higher than 5 $\mu g\,mL^{-1}$ not only when immobilized on a solid surface, but also when in solution.[33] These results are consistent with our findings, since we observed a weak enhancing effect of albumin at much lower concentrations than those used in the previous experiments. Polylysine is a basic polypeptide, which is often used as a general representative for positively charged macromolecules. Polyaspartic acid is an acidic peptide that has been reported to favor the formation of calcium oxalate dihydrate.[34] None of these proteins or peptides had any effect, thus strengthening our conclusion that the observed nucleation effects are not due to nonspecific induction by charge or electrostatic potential.

The interaction between macromolecules extracted from plant crystals and calcium oxalate in vitro was investigated by comparing the morphology of crystals grown in the presence and in the absence of the matrix macromolecules. We showed that macromolecules extracted from crystals isolated from tobacco and tomato specifically inhibit the {120} faces of calcium oxalate monohydrate in vitro. In contrast the macromolecules associated with bougainvillea, which forms raphides (long rod-shaped crystals elongated in [101]), inhibited growth in all directions, yielding rounded crystals with steps on the surface. This may be a result of nonspecific adsorption of macromolecules on calcium oxalate faces, or of the presence of many macromolecules specifically interacting with different crystal surfaces. We noted that specific interactions with the {120} faces occurred only when the oxalate solution was placed in the dialysis bag and not vice versa. We do not understand the reason for this; it could conceivably be related to the conformational and/or aggregation states of the interacting macromolecules, or to the presence of excess oxalate, as opposed to excess calcium, on the growing surfaces of the crystals.

The molecular structures of the $(10\bar{1})$, (102), (101) and of the $(\bar{1}10)$, $(\bar{1}\bar{2}0)$ faces, are shown in Figure 8. The $(10\bar{1})$ face is

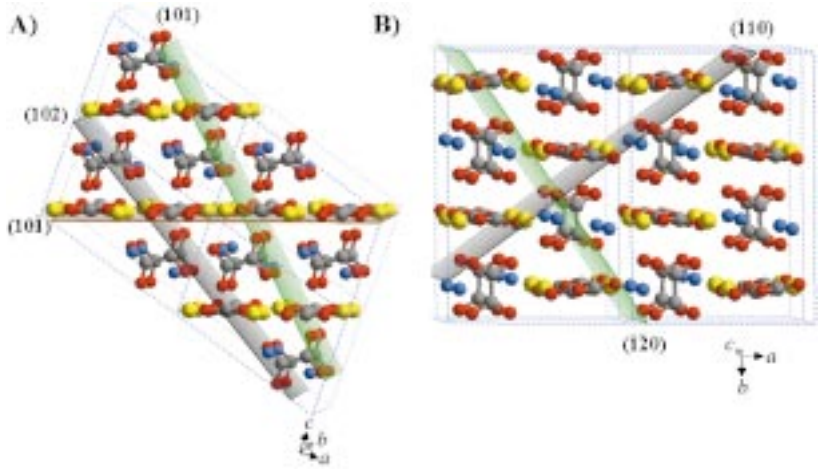

Figure 8. Molecular structure of a COM crystal showing A) $(10\bar{1})$, (102), and (101) faces. B) A different view of the COM crystal showing the $(\bar{1}10)$ and $(\bar{1}\bar{2}0)$ faces. Yellow atoms correspond to calcium, dark grey to carbon, red to oxygen from carboxylates, and blue to oxygen from the water molecules.

characterized by two types of oxalate ions, one emerging oblique to the face and one lying parallel to the face. It is a very stable face, and is thus the main face developed by crystals grown under standard conditions. Either four {120} or four {110} faces are generally developed in control crystals. These are flat faces with balanced charge, where the carboxylates emerge without particular geometrically defined stereochemistry. In a study of mollusk matrix macromolecular interactions with other calcium dicarboxylates, it was shown that specific interactions occur with faces in which the two oxygens of the carboxylate groups emerge perpendicular to the plane of the face such that the coordination polyhedron around the calcium ion can be optimized.[19] These conditions are fulfilled here only in the case of the (101) face, and to a lesser extent by (102). This observation strengthens the suggestion that there is something specific to the faces interacting with the nucleating macromolecules. The growth modulation in vivo may (or may not) be due to different macromolecules that specifically interact with the {120} faces. The in vitro experiments do show that at least some of the crystal-associated macromolecules have conformations that enable them to interact specifically with calcium oxalate crystals as the latter are forming. In vivo they may well function when adsorbed onto the crystal-chamber walls. It is also conceivable that these specifically interacting proteins

0947-6539/01/0709-1886 $ 17.50+.50/0 *Chem. Eur. J.* **2001**, *7*, No. 9

are occluded within the forming crystals on specific planes, and that their function is to alter the mechanical or possibly chemical properties of the crystals.

The importance of calcium oxalate formation in urinary stones has stimulated numerous studies of the effect of synthetic and natural macromolecules on the nucleation, morphology, and growth of calcium oxalate.[28a, 35] However, very little is known about specific interactions of macromolecules with calcium oxalate crystals. Nefrocalcin, an acidic glycopeptide, has been observed to adsorb stereospecifically on the $(\bar{1}01)$ face,[36] and morphological studies of the effect of synthetic glycosaminoglycans on COM showed inhibition of $(\bar{1}01)$ faces.[37] Significantly, specific interactions with the {120} faces were not observed. This may therefore be a unique attribute of calcium oxalate crystal-associated proteins from plants.

Conclusion

The morphologies of calcium oxalate crystals in plants are under genetic control. Here we have shown that, in the case of pseudotetrahedral-shaped crystals, the faces expressed indicate that at least part of this control must be exerted by the microenvironment in which the crystals grow, and is not only a function of the oxalate structure and growth kinetics. The observed chiral morphology of these crystals and the presence in each crystal type of one face that is normally not expressed suggest that control of the nucleation event is of particular importance. Furthermore, the assemblage of macromolecules associated with these crystals is able to promote nucleation in vitro, and to interact specifically with certain faces of the growing crystals. This mode of interaction in vitro is unlikely to reflect the in vivo environment, but does show that the proteins have structures that enable them to interact specifically with calcium oxalate surfaces.

Experimental Section

Materials: Tomato *(Lycopersicon esculentum)* and tobacco (*Nicotiana tabacum)* leaves were collected from the greenhouses of the Department of Plant Sciences, Weizmann Institute of Science. Bougainvillea *(Bougainvillea sp.)* leaves were collected from a local garden. All the samples were collected during winter.

Isolation of calcium oxalate crystals from the leaves: Fresh leaves (approximately 200–300 g) were washed thoroughly with tap water and then with deionized water (DW). They were placed for two hours in a beaker filled with DW containing 1 mM sodium azide, washed, and air-dried. Dry leaves were blended for two minutes in a laboratory blender (Waring) with absolute ethanol (200 mL) to minimize dissolution of the crystals, and the resulting mixture was filtered through four layers of gauze filter. The latter removes the coarse organic fraction. The filtrate was transferred to 50 mL polypropylene centrifuge tubes and centrifuged with absolute ethanol at 4000 rpm (5 min). The supernatant was removed and the pellet was resuspended and vortexed in ethanol. This was repeated twice, and then again three times with DW at 4000 rpm (5 min). The pellet was mixed with sodium polytungstate ($3\,Na\cdot WO_4\cdot 9\,WO_3\cdot H_2O$) (20 mL) of 1.7 g mL^{-1} density and centrifuged three times at 4000 rpm (10 min). The supernatant, together with organic material that does not pellet under these conditions, was discarded and the pellet was resuspended, vortexed, and centrifuged again three times with DW at 3000 rpm (5 min), then with absolute ethanol under the same conditions, and air-dried. If the purity of the crystals was not adequate (as determined by FTIR spectroscopy) the centrifugation with the heavy liquid was repeated using a density of 1.9 g mL^{-1}.

Characterization of calcium oxalate crystals: The isolated crystals were characterized by X-ray powder diffraction (Rigaku D/max-B rotating anode diffractometer with CuKa radiation at 40 kV, and 100 mA) and FTIR spectroscopy (MIDAC, Costa Mesa, CA, USA), with pure synthetic calcium oxalate monohydrate (COM) and calcium oxalate dihydrate crystals (COD) used as standard materials. The synthetic crystals were prepared by procedures described previously,[38] with minor modifications as follows: Pure COM was prepared by the simultaneous dropwise addition of 0.04 M sodium oxalate (250 mL) and 0.04 M calcium chloride (250 mL) into DW (1000 mL) at 75 °C. The rate of addition was approximately 2 mL min^{-1} and the solution was magnetically stirred. The suspension was stirred (2 h), filtered through 0.8 μm Millipore membrane filters and washed with DW. The crystals were dried in a desiccator under vacuum. COD was prepared by the rapid addition (mixing time <2 s) of 0.05 M sodium oxalate (16 mL) into a solution containing 0.01 M sodium citrate (400 mL) and 0.2 M calcium chloride (32 mL). The suspension was stirred (2 min), filtered through 0.8 μm Millipore membrane filters and air-dried.

Dissolution of extracted crystals: Clean, dry crystals (approximately 60–70 mg) were suspended in DW (6 mL) containing 1 mM sodium azide and sonicated (15 min). Equal volumes of suspension were poured into 3 dialysis bags (Spectra/Por; molecular weight cut-off 3500 daltons, diameter 11.5 mm). Each bag was placed in a 50 mL centrifuge tube filled with two-thirds DW and one-third Dowex 50WX8 cation exchange resin (Sigma, H^+ form, mesh 50–100*)* prewashed with deionized water. The tubes were rotated continuously at 18 rpm in a propeller-like mode to allow close contact between the resin and the suspension inside the bag. The DW inside the tube was changed twice a day and the resin was changed every 3 days. After 9–10 days the contents of the bags were mixed and centrifuged at 4000 rpm (5 min). The supernatant was filtered through 0.22 μm membrane filter, dialyzed against four changes of DW over 2 days, and stored at -4 °C for further analysis. In order to reduce the volume (if it was necessary) the sample was concentrated in a vacuum concentrator (Savant Speed Vac) or a lyophilizer.

Amino acid analysis: Aliquots of the soluble matrix were lyophilized and hydrolyzed under vacuum in 6 N HCl (0.3 mL) at 110 °C (22 h) after flushing twice with nitrogen. The mixture of amino acids obtained by hydrolysis was derivatized with AccQ Tag reagent (Waters) and analyzed by reverse-phase separation on an HPLC (Waters 2690).

Morphological analysis of natural crystals:

Scanning electron microscopy: Glass cover slips (diameter 12 mm) were coated with gold on both sides and mounted on an aluminum stub with a double-sided carbon tape. One drop of a very dilute suspension of crystals extracted from the leaves was placed on the slide, air-dried, and sputtered with gold. The crystals were examined in a Jeol 6400 SEM. The specimen was rotated and tilted in turn in positions such that the faces that define each dihedral angle in a single crystal were both edge-on. The dihedral angles were measured from the corresponding SEM micrographs.

Transmission electron microscopy: A small amount of dry crystals was placed in a centrifuge tube containing 100% ethanol (2 mL), vortexed, and sonicated for 2 min. One drop of the suspension was placed on carbon-baked 600 mesh nitrocellulose-coated nickel grids and allowed to settle for 30 s. The supernatant was removed with filter paper and air-dried. The grid was mounted on a cryoholder (Gatan cryotransfer system model 626), inserted into the microscope and cooled to -175 °C with liquid nitrogen. Images and electron diffraction patterns of individual crystals were recorded with a Philips CM120 transmission electron microscope. The thin edges of the crystal were used for electron diffraction. Diffraction patterns from different parts of the same crystal were essentially identical. The spot size of the beam was 1.4 μm. Calibration for d-spacing was performed using a gold standard and correction for axial rotation was performed using a molybdenum trioxide standard.

In vitro assay of protein–calcium oxalate crystal interactions: Crystal formation in vitro was allowed to occur in the presence and in the absence of extracted macromolecules by the diffusion growth technique in two different environments: a calcium-rich environment and an oxalate-rich environment. In the first case, 1.8×10^{-2} M calcium chloride (1.1 mL) containing the additive was placed in a membrane (Spectra/Por 3;

molecular weight cut-off of 3500 daltons, diameter 11.5 mm). The membrane was closed and placed in a 50 mL polystyrene tube containing 5.10^{-4} M sodium oxalate (40 mL). In the second case the oxalate was poured inside the membrane and the calcium was outside, in the same concentrations as previously. Control experiments in the absence of the additives were run in parallel. The tubes were not moved. After three days the suspensions inside and outside the membrane were filtered through 0.22 μm membrane filters and the morphology of the crystals produced was characterized by scanning electron microscopy.

Nucleation assay: Spontaneous precipitation experiments were conducted using the method described by Hennequin et al.[39] with minor modifications. Stock solutions of sodium chloride, sodium oxalate, and calcium chloride were prepared from the corresponding solids (Merck, Pro analysis reagents). Bovine serum albumin, poly(L-aspartic acid) (MW: 5000–15000), and poly(D-lysine) (MW: 4000–15000) were purchased from Sigma. Experiments were carried out at 25 °C, pH 5.5, ionic strength 0.15 M NaCl, and oxalate/calcium molecular ratio 10:1. Briefly, 2 M NaCl (0.15 mL) was mixed with 0.02 M sodium oxalate (0.33 mL) in a polystyrene spectrophotometric cuvette (Sigma) and the appropriate amounts of additive and DW were added to a final volume of 1.67 mL. An aliquot of 0.002 M calcium chloride (0.33 mL) was added to the above solution and the absorbance at 620 nm was monitored with an LKB Biochrom Ultrospec II spectrophotometer. Control experiments without additives were also run. All solutions were filtered twice through 0.22 μm membrane filters before use, and each experiment was repeated 3–5 times. The time elapsed between the creation of the supersaturation and the change in absorbance (620 nm) of the solution is defined as the induction time (t) and the nucleation effect is expressed as t_0/t_1, where t_o is the induction time in a pure solution and t_i the induction time in the presence of the additive.

Acknowledgement

We thank Prof. Robert Fluhr (Department of Plant Sciences, Weizmann Institute of Science) for providing us with the tomato and tobacco leaves. We also thank Dr. E. Beniash and T. Arad for their help with the transmission electron microscope. S.W. is the incumbent of the I. W. Abel Professorial Chair of Structural Biology and L.A. is the incumbent of the Dorothy and Patrick Gorman Professional Chair of Biological Ultrastructure. The research was supported by the Minerva Foundation.

[1] a) T. Pobequin, *Ann. Sci. Nat. Bot. Ser. II* **1954**, *15*, 29–109; b) J. Sachs, in *Textbook of Botany* (Ed.: S. R. Vines), Clarendon Press, Oxford, **1882**; c) L. Ajello, *Amer. J. Bot.*, **1941**, *28*, 589–594; d) H. Arnott, F. Pautard, in *Biological Calcification: Cellular and Molecular Aspects* (Ed.: H. Schraer), Meredith, New York, **1970**, pp. 375–446; e) H. A. Lowenstam, S. Weiner, *On Biomineralization*, Oxford University Press, New York, **1989**; f) V. Franceschi, H. Horner, *Bot. Rev.* **1980**, *46*, 361–427.

[2] a) H. Arnott, in *Biological Mineralization*, (Ed.: Isadore Zipkin), Wiley, New York, **1973**, pp. 609–626; b) K. Simkiss, K. M. Wilbur, in *Biomineralization: Cell Biology and Mineral Deposition*, Academic Press, San Diego, **1989**, pp. 106–130.

[3] M. A. Webb, *Plant Cell* **1999**, *11*, 751–761.

[4] a) E. Stahl, *Z. Naturwiss. Med.* **1888**, *22*, 105; b) W. Sakai, M. Hanson, R. Jones, *Science* **1972**, *178*, 314–315.

[5] D. S. Finley, *Rev. Biol. Trop.* **1999**, *47*, 27–31.

[6] a) R. A. Sterling, *Acta Crystallogr.* **1965**, *18*, 917–921; b) H. Arnott, F. Pautard, H. Steinfink, *Nature* **1965**, *5016*, 1197–1198.

[7] a) A. Frey-Wyssling, *Am. J. Bot.* **1981**, *68*, 130–141; b) A. Cody, H. Horner, *Scanning Electron Microsc.* **1984**, *III*, 1451–1460.

[8] a) V. M. Racicot, C. M. Rinderle, K. G. Ragothama, M. A. Webb, *Plant Physiology* **1997**, *114*, 1641–1641; b) E. Zindler-Frank, *Bot. Acta* **1995**, *108*, 144–148.

[9] V. R. Franceschi, *Protoplasma* **1984**, *120*, 216–223.

[10] H. J. Arnott, in *Biological Mineralization and Demineralization* (Ed.: G. H. Nancollas), Springer, New York, **1982**, pp. 199–218.

[11] a) L. Addadi, S. Weiner, *Angew. Chem.* **1992**, *104*, 159–176; *Angew. Chem. Int. Ed. Engl.* **1992**, *31*, 153–169; b) K. Simkiss, in *Biomineralization in Lower Plants and Animals* (Eds.: B. S. C. Leadbeater, R. Riding), Clarendon Press, Oxford, **1986**, pp. 19–37.

[12] S. Mann, in *Biomineralization, Chemical and Biochemical Perspectives* (Eds.: S. Mann, J. Webb, R. J. P. Williams), VCH, Weinheim, **1989**, pp. 35–60.

[13] A. Berman, L. Addadi, S. Weiner, *Nature* (London), **1988**, *331*, 546–548.

[14] M. A. Webb, J. M. Cavaletto, N. C. Carpita, L. E. Lopez, H. J. Arnott, *Plant* **1995**, *7*, 633–648.

[15] A. Cody, H. Horner, *Am. J. Bot.* **1985**, *72*, 1149–1158.

[16] a) J. Vesque, *Ann. Sci. Nat.(Bot)* **1874**, *19*, 300–313; b) G. Arcangeli, *Bull. Soc. Bot. Ital.* **1891**, *23*, 367–372; c) H. Philipsborn, R. Hodenberg, *Protoplasma* **1958**, *49*, 320–324.

[17] S. Deganello, O. Piro, *N. Jb. Miner. Mh.* **1981**, *2*, 81–88.

[18] D. Worms, S. Weiner, *J. Exp. Zool.* **1986**, *237*, 11–20.

[19] L. Addadi, S. Weiner, *Proc. Natl. Acad. Sci. USA* **1985**, *82*, 4110–4114.

[20] A. Myerson, R. Ginde, in *Handbook of Industrial Crystallization* (Ed.: A. S. Myerson), Butterworth–Heinemann, Boston, **1993**, pp. 33–63.

[21] J. Aizenberg, J. Hanson, T. F. Koetzle, L. Leizerowitz, S. Weiner, L. Addadi, *Chem. Eur. J.* **1995**, *7*, 414–422.

[22] a) S. Mann, N. H. Sparks, R. P. Blakemore, *Proc. R. Soc. Lond.* **1987**, *B231*, 477–487; b) J. M. Didymus, J. R. Young, S. Mann, *Proc. R. Soc. Lond.* **1994**, *B258*, 237–245; c) J. R. Young, J. M. Didymus, P. R. Brown, B. Prins, S. Mann, *Nature* **1992**, *356*, 516–518.

[23] S. Mann, R. B. Frankel in *Biomineralization, Chemical and Biochemical Perspectives* (Eds.: S. Mann, J. Webb, R. J. P. Williams), VCH, Weinheim, **1989**, pp. 389–426.

[24] a) L. Addadi, Z. Berkovitch-Yellin, I. Weissbuch, M. Lahav, L. Leiserowitz, S. Weinstein, *J. Am. Chem. Soc.* **1982**, *104*, 2075–2077; b) J. M. McBride, S. B. Bertman, *Angew. Chem.* **1989**, *101*, 342–345; *Angew. Chem. Int. Ed. Engl.* **1989**, *28*, 330–333; c) I. Weissbuch, L. Addadi, M. Lahav, L. Leiserowitz, *Science* **1991**, *253*, 637–645.

[25] a) A. Wierzbicki, M. Taylor, C. Knight, J. Madura, J. Harrington, C. Sikes, *Biophys. J.* **1996**, *71*, 8–18; b) R. Laursen, D. Wen, C. Knight, *J. Am. Chem. Soc.* **1994**, *116*, 12057–12058.

[26] J. Aizenberg, J. Hanson, T. F. Koetzle, S. Weiner, L. Addadi, *J. Am.Chem. Soc.* **1997**, *119*, 881–886.

[27] S. Albeck, J. Aizenberg, L. Addadi, S. Weiner, *J. Am. Chem. Soc.* **1993**, *115*, 11691–11697.

[28] a) R.L. Ryall, *Pediatr. Nephrol.* **1996**, *10*, 656–666; b) F. Atmani, P. Glenton, S. Khan, *Urol. Res.* **1998**, *26*, 201–207.

[29] J. Aizenberg, G. Lambert, L. Addadi, S. Weiner, *Adv. Mater.* **1996**, *8*, 222–225.

[30] S. Weiner, L. Addadi, *Trends Biochem. Sci.* **1991**, *16*, 252–256.

[31] R. Selvam, P. Kalaiselvi, *BJU Int.* **2000**, *86*, 7–13.

[32] a) W. Wu, D. E. Gerard, G. H. Nancollas, *J. Am. Soc. Nephrol.* **1999**, *10*, S355–S358; b) S. T. Liu, A. Hurwitz, G. H. Nancollas, *J. Urol.* **1982**, *127*, 351–355.

[33] C. Cerini, S. Geider, B. Dussol, C. Hennequin, M. Daudon, S. Veesler, S. Nitsche, R. Boistelle, P. Berthezene, P. Dupuy, A. Vazi, Y. Berland, J. C. Dagorn, J. M. Verdier, *Kidney Int.* **1999**, *55*, 1776–1786.

[34] J. A. Wesson, E. M. Worcester, J. G. Kleinman, *J. Urol.* **2000**, *163*, 1343–1348.

[35] a) K. Bouropoulos, N. Bouropoulos, M. Melekos, P. G. Koutsoukos, G. C. Chitanu, A. G. Anghelescu-Dogaru, A. A. Carpov, *J. Urology* **1998** *159*, 1755–1761; b) A. M. Cody, R. D. Cody, *J. Cryst. Growth* **1994**, *135*, 235–245; c) A. Wierzbicki, C. S. Sikes, J. D. Sallis, J. D. Madura, E. D. Stevens, *Calcif. Tissue Int.* **1995**, *56*, 297–304; d) L. Tunik, L. Addadi, N. Garti, H. Furedi-Milhofer, *J. Cryst. Growth* **1996**, *167*, 748–755.

[36] S. Deganello, *Calcif. Tissue Int.* **1991**, *48*, 421–428.

[37] Y. Shirane, Y. Kurokawa, Y. Sumiyoshi, S. Kagawa, *Scanning Microsc.* **1985**, *9*, 1081–1088.

[38] C. Kontoyannis, N. Bouropoulos, P. Koutsoukos, *Appl. Spectrosc.* **1997**, *51*, 64–67.

[39] C. Hennequin, V. Lalanne, M. Daudon, B. Lacour, T. Drueke, *Urol. Res.* **1993**, *21*, 101–108.

Received: October 5, 2000 [F2780]

  0947-6539/01/0709-1888 $ 17.50+.50/0